Field angle dependence of the remanent magnetization of multifilamentary $Ag/(Pb,Bi)_2Sr_2Ca_2Cu_3O_{10+x}$ tapes: Microstructure and current carrying capability

V. Hussennether, O. Waldmann, and P. Müller
Physikalisches Institut III, Universität Erlangen-Nürnberg, D-91058 Erlangen, Germany

M. Leghissa and H.-W. Neumüller
Siemens AG, Corporate Technology, D-91050 Erlangen, Germany

(Received 29 March 2000)

We measured the dependence of the remanent magnetization of multifilamentary $(Pb,Bi)_2Sr_2Ca_2Cu_3O_{10+x}$ tapes on the angle between tape surface and magnetic field. Remanent magnetization allows one to separate the intergrain and intragrain contributions. The angle dependence of the intergrain magnetization is accurately described by a thin strip model. The intragrain magnetization can be reproduced by regarding the microstructure as an agglomeration of plateletlike grains. The orientation of the grains is described by a Gaussian distribution. Based on this model we develop a comparatively simple method to determine the mean grain alignment within the tapes. A comparison of the grain alignment inferred from magnetization as well as transport measurements provides direct evidence for the presence of a critical angle for Bi-2223 grain boundaries.

I. INTRODUCTION

$(Pb,Bi)_2Sr_2Ca_2Cu_3O_{10+x}$ (Bi-2223) tapes are promising candidates for introducing high-T_c superconductors to tasks in power engineering and magnet technology.[1] At present, long lengths of these tapes, produced by the powder-in-tube process, possess critical current densities j_c of up to 40 $kA\,cm^{-2}$ at a temperature of 77 K in self-field.[1–3] In short samples even critical current densities higher than 70 $kA\,cm^{-2}$ have been reported.[3] It is a major goal for the further tape development to increase the current carrying capability in order to achieve a profitable employment of this technology.

For that, it is essential to understand the current transfer mechanisms within the tapes. So far three models have been proposed for the current paths in the tapes: the brick-wall model,[4] the railway-switch model,[5] and the freeway model.[6] Though these models focus on various types of grain boundaries they all proceed on the assumption that it is the granular microstructure which limits the tape performance.

The microstructure of the tapes consists of plateletlike grains of Bi-2223 with typical extension of 1 μm along their c axis and 10–20 μm along their ab plane.[7] The c axes of the grains are aligned. Their a and b axes appear at random orientations. This special stacking scheme resulted in the classification of the grain boundaries as [001] twist boundaries, [001] and [100] tilt boundaries. The systematic investigation of the structure and properties of these kinds of grain boundaries has been carried out extensively for bicrystals of $YBa_2Cu_3O_{6+x}$ (YBCO) (Ref. 8) and $Bi_2Sr_2CaCu_2O_{8+x}$ (Bi-2212).[9]

The experiments on YBCO [001] tilt grain boundaries at different misalignment angles ζ revealed clearly the presence of a critical angle $\zeta_c^{YBCO} \approx 5° \cdots 10°$ that determines the transition from strong to weak coupling of the grain boundary. Below ζ_c^{YBCO} the grain boundary acts as a strong link. By exceeding the critical angle ζ_c^{YBCO} the intergrain current density drops sharply to almost zero. In YBCO even the [100] tilt and [100] twist boundaries exhibit a similar behavior whereas in Bi-2212 at least for the [001] twist boundaries a misorientation-independent current transfer was observed.

The peculiarities of the preparation of Bi-2223 bicrystals hindered up to now similar experiments for Bi-2223. Therefore it is still unclear whether the results on the YBCO and Bi-2212 bicrystals can be applied to the Bi-2223 grains present in tapes. Thus in order to study the correlation between microstructure and current carrying capability one is dependent of a comprehensive characterization of the tapes. Commonly the current carrying capability is investigated by transport measurements,[10] the microstructure by means of electron microscopy,[11] x rays,[12] and magneto-optics.[13,15]

In this paper we report on remanent magnetization measurements on multifilamentary Bi-2223 tapes. In particular we focus on the dependence of the orientation of the magnetic field. Remanent magnetization is a particular useful magnetic technique since it allows us to separate the intergrain and intragrain magnetizations.[14] We will show explicitly that the intergrain remanent magnetization is correlated to the transport current carrying capability. Furthermore, we present a comparatively simple method to determine the mean grain alignment within the tapes. It is based on the ratio of the intragrain remanent magnetization measured at two different orientations of the magnetic field. A comparison of the grain alignment inferred from magnetization as well as transport measurements provides direct evidence for the presence of a critical angle also for Bi-2223 grain boundaries. We discuss the implications of this observation for the current flow in the tapes.

The paper is organized as follows. In Sec. II we describe some experimental details and discuss the typical measurement procedure. In Sec. III we analyze the intergrain magnetization with regard to the transport properties of the tapes.

TABLE I. Transport properties of the investigated tapes at $T=77$ K in zero external field.

Tape	I_c (A)	j_c (kA cm^{-2})	V (mm^3)
M	12	6.4	3.23
A	37.8	17.5	4.10
B	51.0	22.6	4.32
C	70.7	31.9	3.91
D	32.0	15.9	3.54
E	60.0	25.9	4.02

This is followed in Sec. IV by a quantitative discussion of the intergrain magnetization. In Sec. V we introduce a model for the intragrain magnetization at arbitrary field orientations. In particular, a mean magnetic misalignment angle θ_{mag} is defined. Finally, in Sec. VI we apply the model to Bi-2223 tapes and discuss the relevance of θ_{mag} for the current carrying capability of Bi-2223 tapes.

II. EXPERIMENTAL TECHNIQUES AND MEASUREMENTS

Multifilametary tapes were produced by the powder-in-tube technique as described elsewhere.[2] A typical cross section of a 55-filament tape is given in Ref. 2. Table I lists the transport properties at 77 K in self-field for the investigated tapes. Sample M is a monocore tape, whereas samples A–E are 55-filamentary tapes. They all possess the same superconducting filling factor $V_{Bi\text{-}2223}/V_{tape}=0.25$. Magnetic measurements were performed on about 5-mm-long pieces cut from long lengths of the tapes. The sample volumes V_{tape} as determined by a calliper rule to an accuracy of $(10\ \mu\text{m})^3$ are given in Table I. Magnetic hysteresis loops were measured with a commercial superconducting quantum interference device magnetometer. From these the remanent magnetic moment was determined as function of the maximum applied field H_0. If not stated otherwise, the measurements were performed at temperatures $T=5$ K. The magnetization M was evaluated using the superconducting volume $V_{Bi\text{-}2223}$ of the samples. Magnetic fields were applied with different orientations to the tape plane. The perpendicular configuration corresponds to fields perpendicular to the tape surface. In parallel configuration the magnetic field is parallel to the tape surface and perpendicular to the tape length. The accuracy of the sample alignment was $\pm 0.5°$.

In Ref. 14 it has been shown that the logarithmic derivative of the remanent magnetization $\tilde{M}_{rem} \equiv dM_{rem}/d\log H_0$ allows for a separation of intergrain and intragrain magnetic moments. A bending of the samples to diameters smaller than 2 mm, which destroys the intergranular connections, has been used to investigate separately the intragranular magnetic moments.[16,14]

By means of typical measurements of $\tilde{M}_{rem}$ several aspects of importance for the following discussion will be introduced. In Fig. 1 $\tilde{M}_{rem}$ is plotted for three representative tapes for the perpendicular and parallel configuration. The peak at lower fields is due to the intergranular, the peak at higher fields is due to the intragranular magnetic moment.[14] The curves depend both on the orientation of the magnetic field and on the critical current densities of the tapes. We characterize the peaks by their positions $H_{p,inter}$ and $H_{p,intra}$ and their amplitudes P_{inter} and P_{intra}. Peak positions could be determined with an accuracy of 10%, peak heights with 5%.

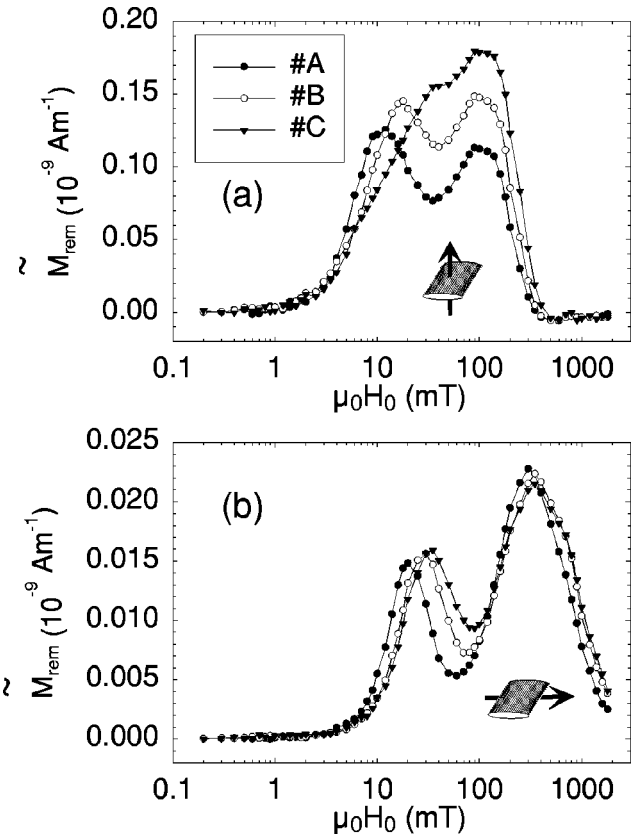

FIG. 1. Logarithmic derivative of the remanent magnetization for the intact samples A, B, and C at $T=5$ K in perpendicular (a) and parallel (b) configuration. Data are normalized to the superconducting volume.

Figure 2 shows $\tilde{M}_{rem}$ for the same samples as in Fig. 1 after being bent strongly. Nevertheless, the intergranular connections are not completely destroyed by the bending procedure since in parallel orientation still an intergrain peak is observable. By comparing the heights of the intergrain peaks for the intact and bent samples [Figs. 1(b) and 2(b)] one finds a suppression of the intergrain magnetization by about a factor of 5.

III. INTERGRAIN AND TRANSPORT CRITICAL CURRENT DENSITIES

The most apparent feature of the intergrain peaks in Fig. 1 is a shift of the peak positions with increasing transport current carrying capability to higher fields. This is further illustrated in Fig. 3 where the critical current density j_c is plotted versus the position of the intergrain peak $H_{p,inter}$ for various tapes. The transport measurements correspond to $T=77$ K, whereas the magnetic properties refer to measurements at $T=5$ K in perpendicular configuration. The tapes with critical current densities smaller than 5 kA/cm^2 stem from intermediate stages of the thermomechanical treatment (after the first heat treatment). The further rolling steps change the aspect

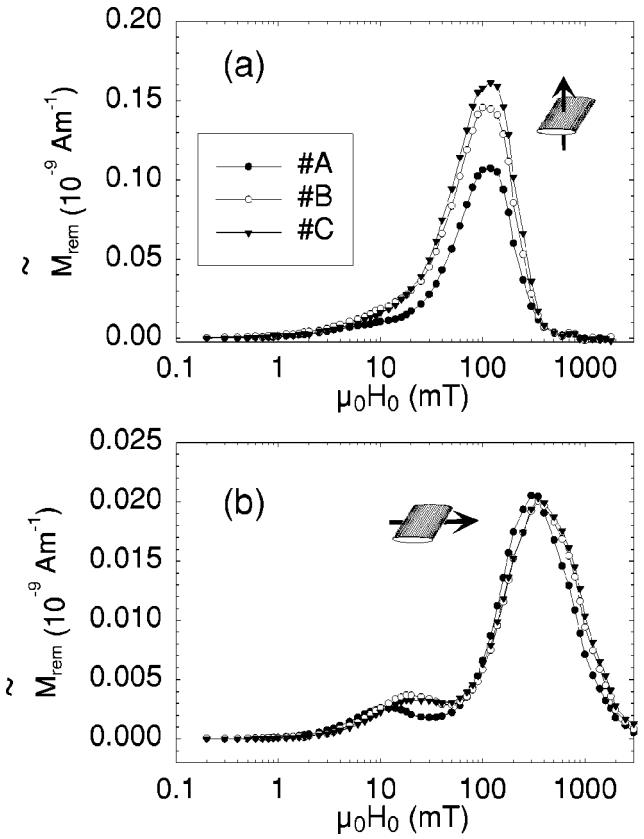

FIG. 2. Logarithmic derivative of the remanent magnetization for samples A, B, and C after being bent strongly, $T=5$ K. (a) perpendicular and (b) parallel configuration for data normalized to the superconducting volume.

ratios of the filaments only by approximately 5%. Therefore these samples can be considered as being similar in geometry as the fully processed tapes.

Figure 3 clearly shows that the position of the intergrain peak $H_{p,inter}$ is correlated with the transport critical current density j_c. $H_{p,inter}$ is directly related to the intergrain characteristic field $H_{c,inter} \propto j_{c,inter} d$, where d denotes the thickness of the filaments (see Sec. IV). Thus in our case where samples with identical geometries are considered the intergrain peak positions are a direct measure of the intergrain critical current densities $j_{c,inter}$.

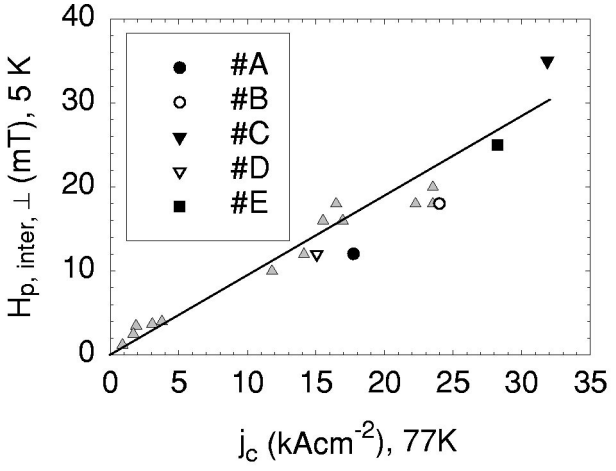

FIG. 3. Correlation between the position of the intergrain peak $H_{p,inter,\perp}$ in perpendicular configuration and j_c. Samples not specified in the legend (grey symbols) originate from tapes with identical geometry as the tapes A–E. The sketched line is a guide to the eye.

Since our study includes samples in different stages of the thermomechanical treatment Fig. 3 shows that both the transport and the intergrain critical current density develop simultaneously during the thermomechanical treatment. For a comparison of the transport and intergrain properties it is important to take into account the typical length scales of the current flow. Magnetically induced currents $j_{c,inter}$ act on a length scale which is comparable to the width of the filaments[14] while transport currents j_c extend over macroscopic length scales. The fact that even fully processed tapes exhibit distinct $j_{c,inter}$ evidences that differences in their microstructure appear on a length scale which is smaller than the filament width. Macroscopic defects, e.g., transversal cracks within the filaments, suppress the transport current but have no effect on the intergrain currents.[14] Such defects lead to a horizontal shift in Fig. 3 and thus to a spread of the data.

IV. DEPENDENCE OF THE INTERGRAIN MAGNETIZATION ON THE ORIENTATION OF THE MAGNETIC FIELD

For analyzing the intergrain magnetization a single filament may be treated as a thin strip with width $2a$, thickness d, and length L ($d \ll a \ll L$). Assuming constant critical current density j_c the formulas for the magnetization are well known. For magnetic fields H applied perpendicular to the strip surface the virgin magnetization is given by[17]

$$M_{virg,\perp}(H) = -\frac{\pi}{4}\epsilon H_{c,\perp} \tanh\frac{H}{H_{c,\perp}}, \tag{1}$$

where $H_{c,\perp} = j_c d/\pi$ is the characteristic field and $\epsilon = 2a/d$ denotes the aspect ratio of the strip.

In parallel configuration the magnetic moment is twice that of a slab with infinte length as has been shown in Ref. 18. One half of the total magnetic moment originates from the currents flowing along the strip, the other half comes from the far-away ends of the strip where the currents perform a U turn. The virgin magnetization can be written as[19]

$$M_{virg,\parallel}(H) = -H_{c,\parallel}\begin{cases} \dfrac{H}{H_{c,\parallel}} - \dfrac{1}{2}\left(\dfrac{H}{H_{c,\parallel}}\right)^2, & 0 \leqslant \dfrac{H}{H_{c,\parallel}} \leqslant 1 \\ \dfrac{1}{2}, & \dfrac{H}{H_{c,\parallel}} \geqslant 1 \end{cases} \tag{2}$$

with $H_{c,\parallel} = j_c d$.

In both cases, the remanent magnetization as function of the maximum applied field H_0 is obtained as

$$M_{rem}(H_0) = M_{virg}(H_0) - 2M_{virg}\left(\frac{H_0}{2}\right). \tag{3}$$

The position and the amplitude of the maximum in the logarithmic derivative $\tilde{M}_{rem} \equiv dM_{rem}/d\log H_0$ is given for perpendicular fields by

$$H_{p,\perp} \approx 2.00 H_{c,\perp}, \quad P_{p,\perp} \approx 0.421\pi\epsilon H_{c,\perp}. \tag{4}$$

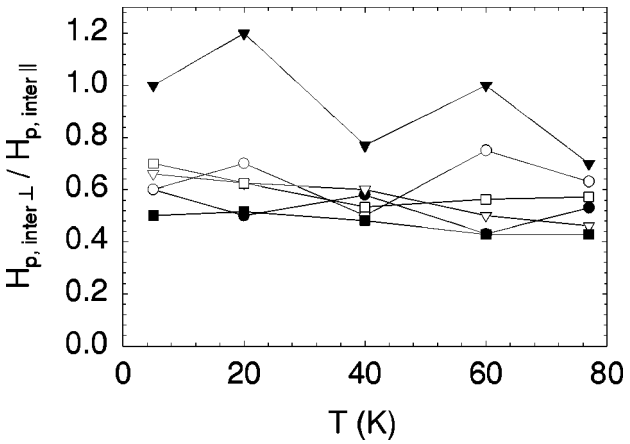

FIG. 4. Ratio of the intergrain peak positions in parallel and perpendicular configuration $H_{p,inter,\parallel}/H_{p,inter,\perp}$ determined in a temperature range of 5–77 K. The plot summarizes data of the monocore tape M (open square) and of the multifilamentary tapes A–E (same legend as is in Fig. 3).

One finds for the position and the amplitude of the maximum for parallel fields

$$H_{p,\parallel}=H_{c,\parallel}, \quad P_{p,\parallel}\approx 1.15H_{c,\parallel}. \tag{5}$$

The filaments within our multifilamentary tapes are arranged in a brick-wall-like stacking scheme.[15] This special configuration allows an external magnetic field to meander around the filaments so that the field pattern around an individual filament in a tape is similar to that of an isolated filament. Consequently, we assume that the total intergranular magnetic moment is the sum of the intergranular magnetic moments of the individual filaments. According to the above equations the major contributions to the intergrain peak of a multifilamentary tape arise from the broad filaments in the central region due to their high critical current densities and aspect ratios.[15]

In the following we extend the considerations for a thin strip to the intergrain magnetization of the tapes. Figure 1 shows that for the multifilamentary tapes $P_{p,inter,\perp}/P_{p,inter,\parallel}\approx 9$. In our tapes the filaments appear with a wide spread of width-to-thickness ratios[15] ranging from 12 to 55 with an average value of 23 which agrees quite nicely with $\epsilon\approx 2.73P_{p,inter,\perp}/P_{p,inter,\parallel}$ found from the peak amplitudes given in Eqs. (4) and (5). Concerning the peak positions one expects from Eqs. (4) and (5) $H_{p,\perp}/H_{p,\parallel}=2/\pi\approx 0.64$. Figure 4 shows the ratio of the peak positions $H_{p,inter,\perp}/H_{p,inter,\parallel}$ for temperatures from 5 K up to 77 K for the tapes of Table I. Figure 4 demonstrates that for all tapes the thin strip result is observed independently of the temperature. Significant deviations appear only for the high-j_c tape C because in the perpendicular configuration the inter- and intragrain peak lie quite close together leading to overestimated peak positions $H_{p,inter,\perp}$ [compare Fig. 1(a)]. It is remarkable that both the monocore and the multifilamentary tapes obey the thin strip result. This confirms our assumption of magnetically independent filaments within one tape. Table II summarizes the temperature dependence of $H_{p,inter,\perp}$ and $H_{p,inter,\parallel}$. The peak positions decrease linearly with increasing temperature in accordance with the linear temperature dependence of the intergrain critical current density $j_{c,inter}$.[20]

TABLE II. Position of the intergrain peak $H_{p,inter}$ for the samples of Table I determined in perpendicular and parallel orientation of the magnetic field.

Tape	5 K (mT)	20 K (mT)	40 K (mT)	60 K (mT)	77 K (mT)
M ⊥	35	25	16	9.0	4.0
M ∥	50	40	25	16	7.0
A ⊥	12	8.0	7.0	3.0	1.6
A ∥	20	16	12	7.0	3.0
B ⊥	18	14	8.0	6.0	2.5
B ∥	30	20	16	8.0	4.0
C ⊥	35	30	14	9.0	3.5
C ∥	35	25	18	9.0	7.0
D ⊥	12	8.0	6.0	3.0	1.4
D ∥	18	16	10	6.0	3.0
E ⊥	25	18	12	6.0	3.0
E ∥	50	35	25	14	7.0

The virgin magnetization curves allow a further test of the thin strip model. Using Eqs. (1) and (2) the initial slope of the virgin magnetization is given by

$$\tilde{M}_{virg,\perp}(0)\equiv dM_{virg,\perp}/dH|_{H\to 0}=-\frac{\pi}{4}\epsilon \tag{6}$$

and

$$\tilde{M}_{virg,\parallel}(0)\equiv dM_{virg,\parallel}/dH|_{H\to 0}=-1, \tag{7}$$

respectively. $\tilde{M}_{virg}(0)$ is thus independent from the superconducting properties. In Fig. 5 $\tilde{M}_{virg}$ is plotted for the monocore tape M and the multifilamentary tape A at $T=5$ K and $T=40$ K for perpendicular and parallel configuration. The data for the parallel configuration show a knee at $\mu_0 H\approx 30$ mT due to the contribution of the intragranular magnetization. For both field configurations the data exhibit saturation to a temperature independent value for $\mu_0 H<1$ mT. The experimentally observed values $\tilde{M}_{virg,\perp}(0)$ for the monocore tape M (-12) and the multifilamentary tape (-19) are nicely consistent with the values calculated from their aspect ratios of $\epsilon=13$ (-10) and $\epsilon=23$ (-18), respectively. Within the experimental accuracy also $\tilde{M}_{virg,\parallel}(0)$ agrees with the thin strip result of -1.

To summarize this section, we have found that the properties of the intergrain magnetization, in particular its dependence on the orientation of the magnetic field, is completely described by the thin strip model. The comparison with the monocore tape showed that the filaments within one multifilamentary tape are not magnetically coupled, at least for dc measurements.

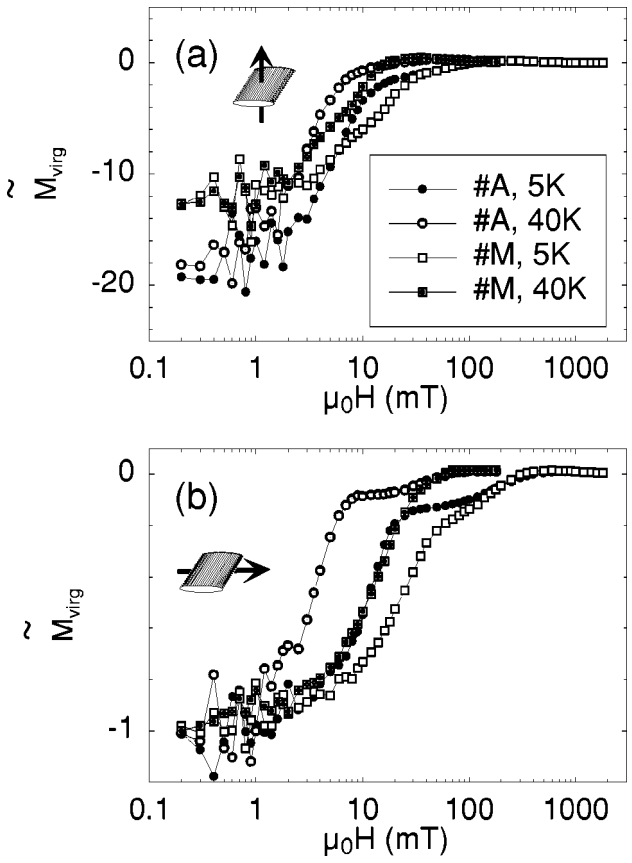

FIG. 5. Slope of the virgin magnetization for the monocore sample M, and the multifilamentary tape A at $T=5$ K and $T=60$ K. (a) perpendicular and (b) parallel configuration for data normalized to the superconducting volume.

V. INTRAGRANULAR MAGNETIZATION OF A TEXTURED MICROSTRUCTURE

In order to describe the intragranular magnetization the microstructure within the filaments may be considered as an agglomeration of Bi-2223 grains. The Bi-2223 grains are approximated by plateletlike cylinders. A microstructure of this kind is shown in Fig. 6(a). This explicit choice for the geometry of the grains is uncritical since the magnetization curves for basic geometries with high aspect ratios, e.g., discs and strips, are very similar.[22] Due to the extreme magnetic anisotropy of Bi-based superconductors the magnetization of the grains is by far dominated by the magnetization within their ab plane.[21]

We first discuss the magnetization of a single grain with radius R_g and thickness d_g with the crystallographic c axis parallel to the cylinder axis ($d_g \ll R_g$). For magnetic fields applied parallel to the cylinder axis the remanent magnetization as function of the maximum applied field H_0 is given by[23]

$$M_{rem,g}(H_0)=A_g H_{c,g}\left[2\arccos\left(\frac{1}{\cosh(\mu/2)}\right)+2\frac{\sinh(\mu/2)}{\cosh^2(\mu/2)}-\arccos\left(\frac{1}{\cosh\mu}\right)-\frac{\sinh\mu}{\cosh^2\mu}\right], \tag{8}$$

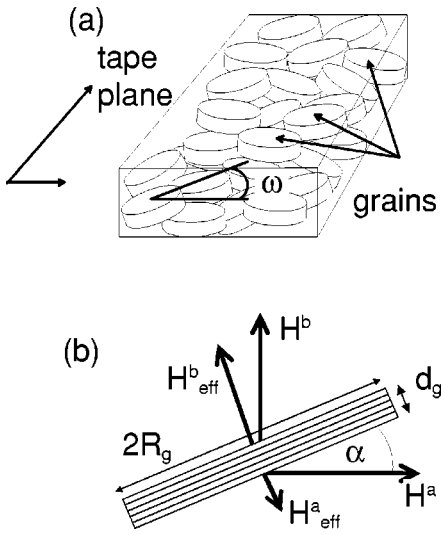

FIG. 6. (a) Shematic sketch of the textured microstructure. The Bi-2223 grains are represented by plateletlike cylinders, for which the orientation is given by a probability distribution of the angle ω. (b) Single anisotropic grain placed in two configurations of the magnetic field H^a and H^b. H^a_{eff} and H^b_{eff} denote the fields that cause the in-plane magnetization.

with $\mu=H_0/H_{c,g}$, $H_{c,g}=j_{c,g}d_g/2$, and $A_g=8R_g/3\pi d_g$. For the logarithmic derivative of Eq. (8) one finds

$$\tilde{M}_{rem,g}(H_0)=(\ln 10)A_g H_0\left[\frac{1}{\cosh^3(\mu/2)}-\frac{1}{\cosh^3(\mu)}\right] \tag{9}$$

The position of the maximum of Eq. (9) is given by $H_{p,g}=1.54H_{c,g}$ with an amplitude of $P_g=1.33A_g H_{c,g}$.

Figure 6(b) shows a cylinder with its orientation characterized by the angle α. Figure 6(b) illustrates further two configurations of the magnetic field H^a and H^b that are perpendicular to each other. The orientation of the cylinder can be determined by comparing the remanent magnetizations measured for the configurations H^a and H^b. For the configuration H^a one finds

$$M^a_{rem,g}(H_0,\alpha)=M_{rem,g}(H_0\sin\alpha)\sin\alpha, \tag{10}$$

with a peak of $\tilde{M}^a_{rem,g}$ at $H^a_{p,g}=H_{p,g}/\sin\alpha$ and amplitude $P^a_g=P_g\sin\alpha$. For configuration H^b, $M^b_{rem,g}$ is given by

$$M^b_{rem,g}(H_0,\alpha)=M_{rem,g}(H_0\cos\alpha)\cos\alpha. \tag{11}$$

$\tilde{M}^b_{rem,g}$ exhibits a peak at $H^b_{p,g}=H_{p,g}/\cos\alpha$ with an amplitude of $P^b_g=P_g\cos\alpha$. Thus the angle α can be determined either from the peak positions or from the peak amplitudes:

$$\tan\alpha=\frac{H^b_{p,g}}{H^a_{p,g}},\quad \tan\alpha=\frac{P^a_g}{P^b_g}. \tag{12}$$

These findings for a single cylinder can be generalized to a textured microstructure of the kind shown in Fig. 6(a). The grain misalignment is described by a probability distribution $F(\omega)$ of the angle ω [Fig. 6(a)] which in our case is assumed to be a Gaussian distribution. Due to the symmetry of the

texture $F(\omega)$ has an average value of 0°, i.e., $F(\omega)$ is fully characterized by its standard deviation σ. The full width at half maximum (FWHM) of $F(\omega)$ is approximately 2.35 σ. Furthermore, we regard the grains to be magnetically isolated so that the total intragrain magnetization M_{intra} is simply the sum of the magnetizations of the cylinders. This appears as a rather crude assumption since any coupling between the grains is neglected. In Sec. VI we show that this approach is useful as long as one restricts its application to the grain alignment. With Θ denoting the angle between the magnetic field and the tape surface the intragrain remanent magnetization of the microstructure is given by

$$M_{rem,intra}(H_0)=\frac{1}{N}\int_0^{\pi/2}\sin|\Theta-\omega|M_{rem,g}(H_0\sin|\Theta-\omega|)\times F(\omega)\sin\omega d\omega, \quad (13)$$

with $N=\int_0^{\pi/2}F(\omega)\sin\omega d\omega$. For the logarithmic derivative of Eq. (13) one finds

$$\tilde{M}_{rem,intra}(H_0)=\frac{1}{N}\int_0^{\pi/2}\sin^2(\Theta-\omega)\tilde{M}_{rem,g}(H_0\sin|\Theta-\omega|)\times F(\omega)\sin\omega d\omega \quad (14)$$

Equations (13) and (14) summarize our above assumptions to a model for the intragrain magnetization for arbitrary orientations Θ of the magnetic field. The remanent magnetization is characterized by three parameters, namely A_g and $H_{c,g}$ of the grains and by σ of the Gaussian distribution. For the perpendicular ($\Theta=90°$) and parallel ($\Theta=0°$) configuration Eqs. (13) and (14) are simplified since $\sin|\Theta-\omega|$ reduces to $\cos\omega$ and $\sin\omega$, respectively.

In analogy to the case of a single cylinder the evaluation of the peaks of Eq. (14) can be used to infer the mean alignment of the grains within the microstructure. We define a mean magnetic misalignment angle θ_{mag} as

$$\theta_{mag}:=\arctan\frac{P_{intra,\parallel}}{P_{intra,\perp}}. \quad (15)$$

In Eq. (15) $P_{intra,\parallel}$ and $P_{intra,\perp}$ denote the intragrain peak amplitudes of $\tilde{M}_{rem}$ observed in parallel and perpendicular orientation. In contrast to the case of a single cylinder we consider only the peak amplitudes and not the peak positions since the experimental determination of the latter is less accurate. The experimental accuracy of θ_{mag} is $\pm 0.5°$ which is mainly due to a possible misorientation when placing the samples in the magnetometer.

To unravel the relevance of the mean magnetic misalignment angle θ_{mag} we modeled different microstructures by varying the standard deviation σ. The mean magnetic misalignment angles θ_{mag} were determined from Eq. (15) by evaluating numerically the intragrain peak amplitudes $P_{intra,\parallel}$ and $P_{intra,\perp}$ of Eq. (14).

The parameter A_g which corresponds to the aspect ratio R_g/d_g of the grains is of no relevance for θ_{mag} since it cancels in the fraction of Eq. (15), the parameter $H_{c,g}$ ($\propto j_{c,g}d_g$) shifts the intragrain peaks, but affects almost not at all the ratio of the peak amplitudes. The solid line in Fig. 7 shows the relative deviation ($\theta_{mag}/\sigma-1$) of θ_{mag} and σ in the range $3<\sigma<20°$. Apparently, θ_{mag} follows σ with a deviation smaller than 5%. Therefore θ_{mag} is adequate to determine σ unaffected by A_g and $H_{c,g}$.

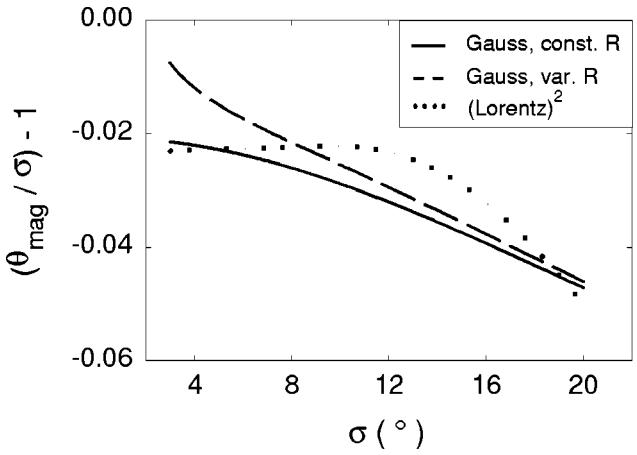

FIG. 7. Relative deviation ($\theta_{mag}/\sigma-1$) versus σ. θ_{mag} was calculated for the modeled microstructure [Fig. 6(a)] using Eqs. (14) and (15).

The assumption of grains with identical geometry is of course a grossly simplified model of the complex microstructure of the tapes. In a more realistic picture one should consider a grain size which decreases with increasing tilt angles ω since the preparation induces the formation of large extended Bi-2223 platelets within the tape plane. We have modeled a variable radius of the grains by a constant $H_{c,g}$ and a varying A_g of the cylinders. A linear decrease of the grain size is assumed with increasing tilt angle ω. Since $A_g=A_g(\omega)$ in this case θ_{mag} is not independent of the grain size, contrary to the constant grain size assumed above. The dashed line in Fig. 7 represents ($\theta_{mag}/\sigma-1$) for a grain size that decreases by a factor of 2 as ω varies from 0 to 2σ. The resulting θ_{mag} differs from θ_{mag} obtained for identical grains by less than 2%. This shows the weak influence of the grain radius on θ_{mag}. Similar results have been obtained for a varying thickness of the grains.

An alternative to the Gaussian distribution is the squared Lorentzian curve used in Ref. 12. For this distribution the FWHM is given by 1.29 δ, where 2δ is the FWHM of the standard Lorentzian. In Fig. 7 the dotted line reflects θ_{mag} determined for the squared Lorentzian distribution as a function of $\sigma=\frac{1.29}{2.35}\delta$. Figure 7 shows that the relative deviation for the squared Lorentzian distribution falls within the range for the Gaussian distribution.

The above discussion shows that neither the geometry of the grains nor the explicit shape of $F(\omega)$ has a significant influence on θ_{mag} determined from the ratio of the intragrain peak amplitudes. Therefore in the following we use a constant grain size and a Gaussian distribution.

VI. RESULTS AND DISCUSSION OF THE INTRAGRAIN MAGNETIZATION

In order to test the validity of the model developed in Sec. V we measured the remanent magnetization at various orientations of the magnetic field. For the tapes the intermixture of the intergrain and intragrain peaks in $\tilde{M}_{rem}$ has to be consid-

ered. In order to determine the heights of the intragrain peaks accurately the measurements have to be performed on bent samples. We investigated the intragrain peak of the low-j_c tape D and the high-j_c tape E at angles Θ of 90, 60, 45, 30, and 0°.

Figure 8 shows that for all orientations the positions of the intragrain peaks do not differ significantly between the samples. In perpendicular configuration, the peaks occur at 100 mT, and are shifted with decreasing angle Θ continuously to higher fields. In parallel configuration the peaks are observed at 300 mT. Also the peak amplitudes exhibit an orientation dependence. The maximal peak amplitudes are observed in perpendicular configuration. By decreasing the angle Θ a suppression of the peak amplitudes occurs. This behavior of the intragrain peaks is in full accordance with our model developed in Sec. V. Since the grains are aligned to the tape surface the magnetic field that is effectively acting on the grains becomes smaller with decreasing angle Θ, thus explaining the shift of the peak position. At the same time the component of the magnetic moment pointing parallel to the external magnetic field becomes smaller, which results in the decreasing peak amplitudes.

For a more rigorous test of the model the measured data were fitted to Eq. (14). Since the model focuses on the characteristics of the peaks the peak amplitudes were stronger weighted by the fitting routine than the peak flanks. We fitted separately the curves for each orientation. In Table III we give the average values for the three parameters and their spread. Table III also shows the experimentally determined θ_{mag} and aspect ratios $2R_g/d_g$ calculated from A_g. In Fig. 8 the lines were calculated for the values given in Table III.

With respect to the peak amplitudes and positions the fit shows an excellent accordance with the measured data. This indicates that our model is truly capable of describing the peaks for variable orientations of the magnetic field. Even the shapes of the peaks are reasonably approximated. This implies that $\tilde{M}_{rem}$ for arbitrary orientations of the magnetic field is fully characterized by only three parameters: A_g and $H_{c,g}$ which are related to the aspect ratio and the characteristic field of the grains, and σ which determines the mean alignment of the grains.

Significant deviations of the fitting curves appear only at the increasing flanks of the intragrain peaks, where the measured data increases stronger than the fit curves. This effect is most pronounced in the perpendicular configuration, whereas in parallel configuration the fit agrees well over the entire range. The deviations arise from the remaining intergrain peak of the bent samples. For the parallel configuration ($\Theta = 0°$) the intergrain and intragrain peaks are clearly separated. With increasing Θ the intergrain peak is shifted towards the intragrain peak resulting in a broadening of the left intragrain peak flank.

In Table III the calculated aspect ratios of 38 for sample D and 47 for samples E overestimate the typical grain dimensions observed in scanning electron microscope (SEM) analysis.[7] This is not unexpected as we assumed magnetically independent grains. The presence of grain clusters can result in intragrain currents acting on a length scale that is larger than the grain size observed in the SEM. Also, nonsuperconducting voids lead to an inaccuracy of the superconducting volume and thus to overestimated aspect ratios.

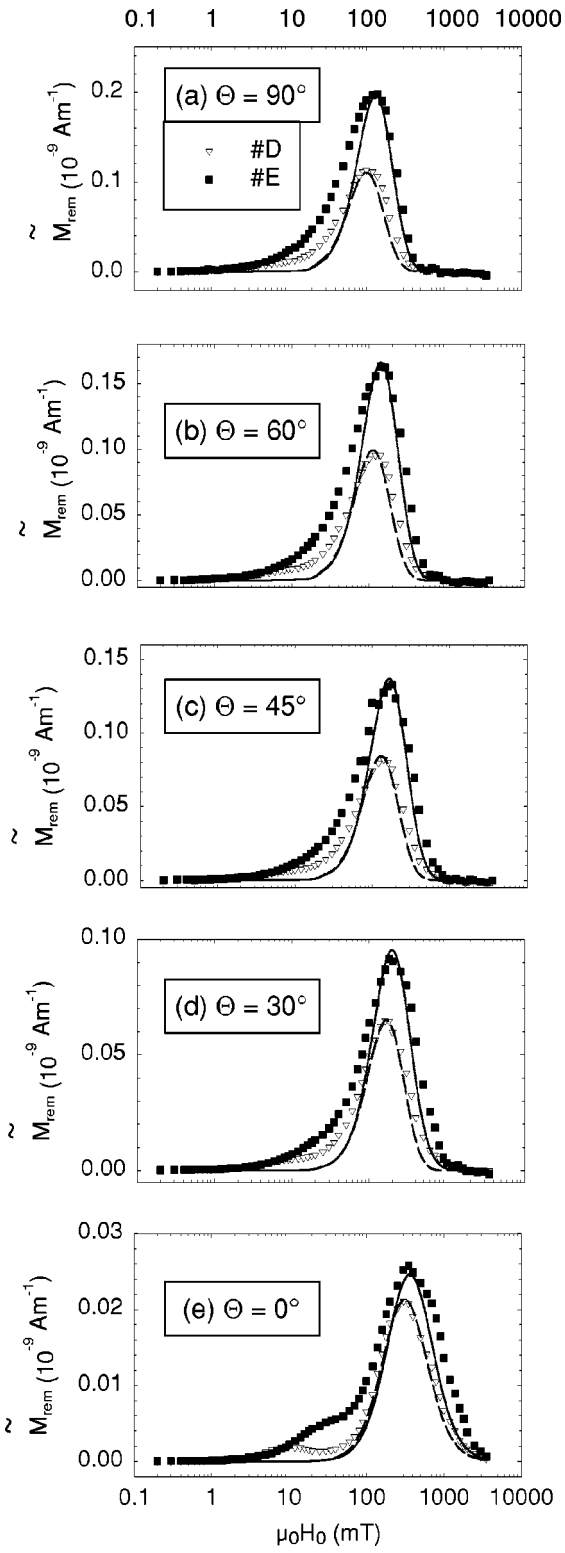

FIG. 8. Logarithmic derivative of the remanent magnetization for bent samples D and E at $T = 5$ K. The measurements were performed at various orientations of the magnetic field ranging from perpendicular (a) to parallel (e) configuration. The lines represent a fit to the measured data using Eq. (14).

Using $H_{c,g} \approx$ 65 mT and assuming a thickness of the grains of 1 μm an intragrain critical current density of approximately 10^4 kA cm^{-2} is estimated from $H_{c,g} = j_{c,g} d_g/2$. This value appears as a reliable estimate since it falls within the experimental results on Bi-2212 crystals given in the

TABLE III. Fitting parameters A_g, $H_{c,g}$, and σ for modeling $\tilde{M}_{rem,intra}(H_0)$ for samples D and E shown in Fig. 8. Values for the calculated aspect ratios $2R_g/d_g$ and the experimentally determined θ_{mag} are also given.

Tape	A_g	$H_{c,g}$ (mT)	σ (°)	$2R_g/d_g$	θ_{mag} (°)
D	16.1±0.2	64.7±0.9	11.3±0.3	38.1±0.4	10.6±0.5
E	20.0±0.2	63.4±1.0	7.6±0.2	47.2±0.5	7.4±0.5

literature.[9] The standard deviations σ differ significantly for the samples. As expected σ determined from the fit agrees well with θ_{mag} derived from $P_{intra,\parallel}$ and $P_{intra,\perp}$.

In order to study the relationship between current carrying capability and grain alignment the mean magnetic misalignment angles were determined on bent samples for a variety of tapes. These tapes were throughout prepared by identical thermomechanical treatments. In Fig. 9 θ_{mag} is plotted versus j_c. A clear correlation appears between θ_{mag} and j_c with a decreasing θ_{mag} accompanied by an increasing j_c.

This observation should not depend on the means of texture analysis so that similar results are expected from a complementary study by x-ray scattering. A detailed texture analysis by x-ray scattering is presented in Ref. 12 for Bi-2223 tapes with a different preparation than our samples but with comparable j_c values. For these tapes a dependence of j_c on the grain alignment similar to ours has been reported by T. R. Thurston *et al.*[12] Remarkably, even a reasonable quantitative accordance is obtained. The FWHM of our Gaussian distribution is approximately 2.35σ so that θ_{mag} ranging from 7 to 12° falls within the FWHM of 20–30° found by Thurston *et al.*[12]

In the following the magnetically determined grain alignment is compared with the results of transport measurements. The mean transport misalignment angles θ_{trans} are derived from the $I_c(B)$ characteristics in parallel and perpendicular configuration. Following S. Kobayashi *et al.* θ_{trans} was determined with an accuracy of ±0.5° for four of the samples shown in Fig. 9, including also the high-j_c and the low-j_c tapes.[10] Independent of their current carrying capability a universal θ_{trans} of 8° was found.

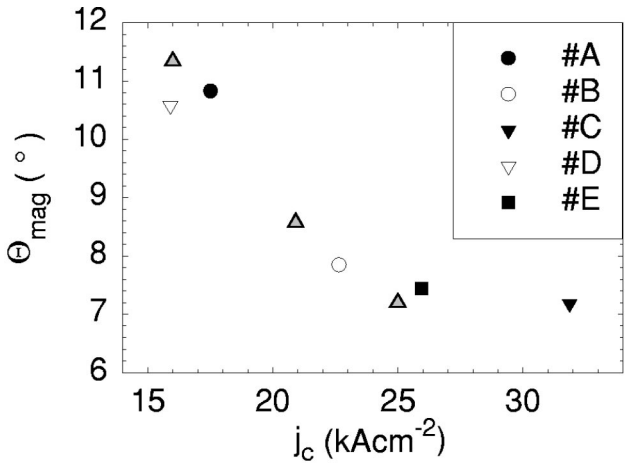

FIG. 9. Mean magnetic misalignment angle θ_{mag} versus j_c for a variety of investigated tapes. Samples that are not specified in the legend (grey symbols) originate from tapes with identical processing as the tapes A–E.

This observation is in striking contrast to the observed magnetic misalignment angles ranging from 7 to 12°. For clarification we consider the differences between these two kinds of measurements. The magnetization represents the sample volume, i.e., all Bi-2223 grains contribute to the measured magnetization. Therefore θ_{mag} represents an overall average value of the tilts of individual grains. θ_{mag} is thus sensitive to both [001] and [100] tilt grain boundaries. [001] twist grain boundaries are not reflected by θ_{mag}. In case of transport only the well joined grains contribute to the current flow. Accordingly, θ_{trans} represents the current transfer at any kind of well joined grain boundary.

If we now assume that $j_{c,inter}$ of the grain boundaries has only a weak dependence on the tilt angle between adjacent grains, then also for the transport all tilt grain boundaries should contribute. Therefore a better alignment of the grains results in a decrease of both θ_{mag} and θ_{trans}. This contradicts our observation of a constant θ_{trans} and significantly decreasing θ_{mag}. Therefore the grain alignment must have a strong impact on the intergrain critical current density.

This suggests a critical angle $\zeta_c^{Bi\text{-}2223}$ that determines the intergrain critical current density $j_{c,inter}$ at the [001] and the [100] tilt grain boundaries in analogy with the misorientation depended behavior in YBCO. Below $\zeta_c^{Bi\text{-}2223}$ the grain boundary acts as a strong link. By exceeding $\zeta_c^{Bi\text{-}2223}$ $j_{c,inter}$ drops sharply to zero. Thereby $\zeta_c^{Bi\text{-}2223}$ is not necessarily identical for the both kinds of tilt grain boundaries. Nevertheless, the tilt grain boundaries of the microstructure can be divided into those with $\zeta < \zeta_c^{Bi\text{-}2223}$ and $\zeta > \zeta_c^{Bi\text{-}2223}$. The difference of θ_{trans} and θ_{mag} is a measure for these two fractions. Transport measurements reflect only the part of the grains with tilt grain boundaries smaller than $\zeta_c^{Bi\text{-}2223}$. That is, constant θ_{trans} will be observed. Thus a critical angle $\zeta_c^{Bi\text{-}2223}$ for the intergrain current transfer naturally explains all our experimental observations.

Clearly, $\zeta_c^{Bi\text{-}2223}$ for Bi-2223 will vary from that in YBCO. As for the bicrystals $\zeta_c^{Bi\text{-}2223}$ will be determined by the specific chemical structure of the tilt grain boundaries. From that a dependence of $\zeta_c^{Bi\text{-}2223}$ on the preparation of the samples is expected. But for our samples with identical processing the transport measurements indicate that $\zeta_c^{Bi\text{-}2223} \approx 8°$.

With these findings we can now also explain the observed scaling of the magnetic field dependence of the transport critical current $I_c(B)$ of the tapes investigated in Ref. 14. It has been found that $I_c(B)/I_c(B_0)$ with $B_0 > 100$ mT is equal for all the tapes. This can be expressed as $I_c(B) = A_{eff} j_{c,uni}(B)$ where $j_{c,uni}(B)$ has been interpreted as a universal intrinsic critical current density and A_{eff} as an effective superconducting area differing for the tapes. The

sharp falloff of $j_{c,inter}(\zeta)$ at $\zeta=\zeta_c^{Bi\text{-}2223}$ tells that all grain boundaries with $\zeta<\zeta_c^{Bi\text{-}2223}$ have similar critical current densities. This directly suggests a universal $j_{c,inter}$. The varying A_{eff} then reflects the specific amount of grain boundaries with $\zeta<\zeta_c^{Bi\text{-}2223}$.

During preparation of this manuscript Cimberle *et al.* published a study on the grain alignment in unreacted tapes.[24] They determined a mean grain alignment from a scaling of hysteresis loops measured in different orientations of the magnetic field. Our results show that even in fully processed tapes, where additionally an intergrain magnetization has to be considered, remanent magnetization measurements are a useful tool to investigate the grain alignment.

VII. CONCLUSIONS

Summarizing, we presented a quantitative study of the intergrain and intragrain magnetization of multifilamentary Bi-2223 tapes at various orientations of the magnetic field. We found that the intergrain magnetization is completely described by a stack of magnetically independent thin strips. Describing the textured microstructure by plateletlike grains with a Gaussian distribution of tilt angles we could accurately reproduce the orientation dependence of the intragrain magnetization. We carefully discussed the applicability of this model with regard to the simplifying assumptions of individual grains and of a Gaussian grain alignment. In particular we showed that the mean grain alignment can be determined from the intragrain magnetization measured at two different orientations of the magnetic field. It is noticeable that this method, in contrast to conventional means of texture analysis, requires no expendable specimen preparation, i.e., only a bending of the samples is needed.

Our investigations of the remanent magnetization revealed several aspects of the current flow in Bi-2223 tapes. Irrespective of the different length scales of current flow the intergrain and transport critical current densities are correlated. Furthermore, our study pointed out the dominating influence of the grain alignment on the current carrying capability of Bi-2223 tapes. A comparison with the grain alignment determined by transport measurements provided the first direct experimental evidence for a critical angle which governs the crossover from strong to weak link behavior of the [001] and [100] tilt grain boundaries. Thus, the mechanisms of current flow in Bi-2223 tapes exhibit a remarkable similarity to the misorientation dependent intergrain current transfer in YBCO bicrystals.

ACKNOWLEDGMENTS

The authors would like to thank B. Fischer and T. Arndt for providing the Bi-2223 tapes. This work has been financially supported by the Bundesministerium für Bildung, Wissenschaft, Forschung und Technologie (BMBF).

[1] M. Leghissa, J. Rieger, J. Wiezoreck, H.-P. Kraemer, B. Roas, B. Fischer, K. Fischer, and H.-W. Neumüller, Inst. Phys. Conf. Ser. **158**, 1191 (1997).

[2] B. Fischer, S. Kautz, M. Leghissa, H.-W. Neumüller, and T. Arndt, IEEE Trans. Appl. Supercond. **9**, 2480 (1999).

[3] A.P. Malozemoff, W. Carter, S. Fleshler, L. Fritzemeier, Q. Li, L. Masur, P. Miles, D. Parker, R. Parrella, E. Podtburg, G.N. Riley, Jr., M. Rupich, J. Scudiere, and W. Zhang, IEEE Trans. Appl. Supercond. **9**, 2469 (1999).

[4] L.N. Bulajevski, J.R. Clem, L.I. Glazman, and A.P. Malozemoff, Phys. Rev. B **84**, 2545 (1992).

[5] B. Hensel, J.-C. Grivel, A. Jerimie, A. Perin, A. Pollini, and R. Fluekiger, Phys. Rev. B **51**, 15 456 (1995).

[6] G.N. Riley, Jr., A.P. Malozemoff, Q. Li, S. Fleshler, and T.G. Holesinger, JOM **49**, 24 (1997).

[7] A. Goyal, E.D. Specht, D.M. Krueger, T.A. Mason, D.J. Dingley, G.N. Riley, and M.W. Rupich, Appl. Phys. Lett. **66**, 2903 (1995); Y. Zhu, M. Suenaga, and R.L. Sabatini, *ibid.* **65**, 1832 (1994).

[8] D. Dimos, P. Chaudhari, and J. Mannhart, Phys. Rev. Lett. **61**, 219 (1988); Phys. Rev. B **41**, 4038 (1990); N.F. Heinig, R.D. Redwing, J.E. Nordman, and D.C. Larbalestier, *ibid.* **60**, 1409 (1999).

[9] Y. Zhu, Q. Li, Y.N. Tsay, M. Suenaga, G.D. Gu, and N. Koshizuka, Phys. Rev. B **57**, 8601 (1998).

[10] S. Kobayashi, T. Kaneko, T. Kato, J. Fujikami, and K. Sato, Physica C **258**, 336 (1996); S. Kobayashi, T. Kaneko , T. Kato, and K. Sato, *Advances in Superconductivity VIII* (Springer, New York, 1996), p. 803; G. Grasso, B. Hensel, A. Jeremie, and R. Flükiger, Physica C **241**, 45 (1995).

[11] T.G. Holesinger, J.F. Bingert, J.O. Willis, Q. Li, R.D. Parella, M.D. Teplisky, M.W. Rupich, and G.N. Riley, Jr., IEEE Trans. Appl. Supercond. **9**, 2440 (1999); O. Eibl, Supercond. Sci. Technol. **8**, 833 (1995).

[12] H.F. Poulsen, T. Frello, N.H. Andersen, M.D. Bentzon, and M.v. Zimmermann, Physica C **298**, 265 (1997); T.R. Thurston, U. Wildgruber, N. Jisrawi, P. Haldar, M. Suenaga, and Y.L. Wang, J. Appl. Phys. **79**, 3122 (1996).

[13] A.E. Pashitski, A. Gurewich, A.A. Polyanski, D.C. Larbalestier, A. Goyal, E.D. Specht, D.M. Kroeger, J.A. DeLuca, and J.E. Tkaczyk, Science **275**, 367 (1997); A.E. Pashitski, A.A. Polyanski, A. Gurewich, J.A. Parell, and D.C. Larbalestier, Appl. Phys. Lett. **67**, 2720 (1995); U. Welp, D.O. Gunter, G.W. Crabtree, W. Zhong, U. Balachandran, P. Haldar, R.S. Sokolowski, V.K. Vlasko-Vlaso, and V.I. Nikitenko, Nature (London) **367**, 44 (1995).

[14] C. Reimann, O. Waldmann, P. Müller, M. Leghissa, and B. Roas, Appl. Phys. Lett. **71**, 3287 (1997).

[15] T. Schuster, H. Kuhn, A. Weisshardt, H. Kronmüller, B. Roas, O. Eibl, M. Leghissa, and H.W. Neumüller, Appl. Phys. Lett. **69**, 1954 (1996).

[16] K.-H. Mueller, C. Andrikidis, H.K. Liu, and S.X. Dou, Phys. Rev. B **50**, 10 218 (1994).

[17] E.-H. Brandt and M. Indenbom, Phys. Rev. B **48**, 12 893 (1993).

[18] E.-H. Brandt, Phys. Rev. B **54**, 4246 (1996).

[19] C.P. Bean, Phys. Rev. Lett. **8**, 250 (1962); C.P. Bean, Rev. Mod. Phys. **36**, 31 (1964).

[20] M.R. Cimberle, A. Canesi, C. Federghini, and A. Grasso, Super-

cond. Sci. Technol. **12**, 460 (1999).
[21] F. Steinmeyer, R. Kleiner, P. Müller, H. Müller, and K. Winzer, Europhys. Lett. **25**, 459 (1994).
[22] E.-H. Brandt, Phys. Rev. B **55**, 14 513 (1997).
[23] J. Zhu, J. Mester, J. Lockhart, and J. Turneaure, Physica C **212**, 216 (1993).
[24] M.R. Cimberle, C. Federghini, G. Grasso, I. Pallecchi, M. Putti, and A.S. Siri, Appl. Phys. Lett. **76**, 85 (2000).